

1 **Tau assemblies do not behave like independently acting prion-like particles in mouse**  
2 **neural tissue**

3

4 Aamir S. Mukadam<sup>\*1</sup>, Lauren V. C. Miller<sup>\*1</sup>, Claire S. Durrant<sup>2</sup>, Marina J. Vaysburd<sup>3</sup>, Taxiarchis  
5 Katsinelos<sup>1</sup>, Benjamin J. Tuck<sup>1</sup>, Sophie Sanford<sup>1</sup>, Olivia Sheppard<sup>2</sup>, Claire Knox<sup>3</sup>, Shi Cheng<sup>1</sup>,  
6 Leo C. James<sup>3</sup>, Michael P. Coleman<sup>2</sup>, William A. McEwan<sup>1,5</sup>

7

8 \* these authors contributed equally to this work

9

10 <sup>1</sup> UK Dementia Research Institute at the University of Cambridge, Department of Clinical  
11 Neurosciences, Cambridge, UK

12 <sup>2</sup> John van Geest Centre for Brain Repair, University of Cambridge, Cambridge, UK

13 <sup>3</sup> MRC Laboratory of Molecular Biology, Francis Crick Avenue, Cambridge, UK

14 <sup>4</sup> Centre for Discovery Brain Sciences, University of Edinburgh, Edinburgh, UK

15 <sup>5</sup> For correspondence: [wm305@cam.ac.uk](mailto:wm305@cam.ac.uk)

16

17 **Abstract**

18 A fundamental property of infectious agents is their particulate nature: infectivity arises from  
19 independently-acting particles rather than as a result of collective action. Assemblies of the  
20 protein tau can exhibit seeding behaviour, potentially underlying the apparent spread of tau  
21 aggregation in many neurodegenerative diseases. Here we ask whether tau assemblies share  
22 with classical pathogens the characteristic of particulate behaviour. We used organotypic  
23 hippocampal slice cultures from P301S tau transgenic mice in order to precisely control the  
24 concentration of extracellular tau assemblies. Whilst untreated slices displayed no overt signs  
25 of pathology, exposure to tau assemblies could result in the formation of intraneuronal,  
26 hyperphosphorylated tau structures. However, seeding ability of tau assemblies did not titrate  
27 in a one-hit manner in neural tissue. The results suggest that seeding behaviour of tau only  
28 arises at supra-physiological concentrations, with implications for the interpretation of high-

29 dose intracranial challenge experiments and the possible contribution of seeded aggregation

30 to human disease.

31

32

### 33 **Introduction**

34 Neurodegenerative diseases are typified by the accumulation of specific proteins into fibrillar  
35 assemblies. In around twenty distinct neurodegenerative diseases, including the most  
36 common, Alzheimer's disease, the protein tau forms hyperphosphorylated, filamentous  
37 inclusions within the cytoplasm of neurons. Evidence from human genetics suggests that tau  
38 accumulation can be a direct cause of neurodegeneration since around 50 distinct mutations  
39 in *MAPT*, the gene that encodes tau, cause inherited forms of dementia with evidence of tau  
40 filaments [1]. The origin of tau assemblies in the human brain remains uncertain. Cell-  
41 autonomous processes may lead to the spontaneous nucleation of oligomeric forms of tau  
42 within the cytoplasm of neurons. Some of these assemblies adopt filamentous conformations  
43 that are able to undergo extension by the addition of tau monomers to the filament ends. Over  
44 the past decade it has been postulated that, in addition to these cell-autonomous mechanisms,  
45 tau pathology may occur through a spreading or prion-like mechanism [2]. Several lines of  
46 evidence demonstrate that assemblies of tau can be taken up into cells, whereupon they seed  
47 the conversion of native tau to the assembled state. Addition of tau assemblies to the exterior  
48 of cells, or the injection of tau assemblies to the brains of tau-transgenic mice, can induce  
49 intracellular tau assembly in the recipient [3–5].

50

51 Population cross-sectional studies demonstrate that tau pathology follows a predictable  
52 pattern over time and space in the human brain consistent with spreading, potentially via a  
53 prion-like mechanism. Immunoreactivity to antibodies such as AT8, which detects tau that is  
54 abnormally phosphorylated at positions S202 and T205 [6], progresses in a manner that can  
55 be systematically categorised into stages according to anatomical distribution (Braak stages  
56 0 - VI) [7,8]. In young adults, some AT8 immunoreactivity is observed in the vast majority of  
57 brains by the third decade of life. However, it is generally confined to neurons within the locus  
58 coeruleus (LC) in the brainstem (Braak pretangle stages 0 a-c and 1a,b). Subsequently, AT8  
59 staining is observed in the entorhinal cortex (EC) and hippocampus (HC) (Braak stages I-II).  
60 Later stages are characterised by progressive dissemination and increasing density of staining  
61 in neocortical regions (Braak stages III-VI). These late stages are associated with severe

62 disease and the overall burden of tau pathology negatively correlates with cognitive function  
63 [9].

64

65 Though intracranial challenge experiments demonstrate that seeded aggregation can in  
66 principle occur, they provide little insight as to whether physiological concentrations of  
67 extracellular tau species might support prion-like activity. The concentration of tau in wildtype  
68 mouse interstitial fluid (ISF) is around 50 ng/ml total tau (equivalent to ~1 nM tau monomer).  
69 Mouse ISF levels typically exceed cerebrospinal fluid (CSF) tau levels by around 10-fold [10].  
70 In humans between ages 21 to 50 years, CSF total tau is below 300 pg/mL increasing to 500  
71 pg/mL over age 70 [11] – approximately 7 to 12 pM if considering the average mass of full  
72 length tau isoforms. Levels are increased 2-3 fold in Alzheimer’s disease [12]. If a similar  
73 relationship between ISF and CSF tau concentration exists in humans as in mice, ISF tau  
74 levels are likely in the order of 100 pM, rising to 300 pM in Alzheimer’s disease. Intracranial  
75 injection experiments typically supply tau in the high micromolar range. Even if this were  
76 distributed broadly across the brain, micromolar concentrations would be exceeded and local  
77 concentration at the injection site may plausibly be 100-fold greater. Thus, intracranial injection  
78 experiments likely exceed physiological concentrations of extracellular tau by two to seven  
79 orders of magnitude.

80

81 For classical infectious agents, infectivity is related to dose by a “one-hit” relationship wherein  
82 the amount of infectivity decreases linearly upon dilution until end-point [13]. This property is  
83 also evident in PrP<sup>Sc</sup> prions, though it is complicated by the presence of multiple aggregation  
84 states and the size distribution of particles [14]. The relationship between dose and prion-like  
85 activity for tau has not been established. It is therefore currently not possible to reconcile high-  
86 dose challenge experiments with the low concentrations of tau observed in the extracellular  
87 spaces of the brain. To address this, we developed a model of seeded tau aggregation in  
88 mouse organotypic hippocampal slice cultures, allowing direct control of the concentration of  
89 tau neurons were exposed to. Brain slice cultures have been used for 40 years [15], though



90 developments in recent years have rendered them increasingly relevant for the study of  
91 neurodegenerative diseases [16–20]. We prepared slices from transgenic mice with the *MAPT*  
92 P301S mutation [21], which is causative of fronto-temporal dementia and displays accelerated  
93 fibrilisation compared to wildtype tau [22]. ISF concentrations of tau in P301S transgenic mice  
94 have previously been measured at about 5 times that of wildtype animals at around 5 nM  
95 monomer equivalent, versus 1 nM in wildtype, consistent with the reported 5-fold over-  
96 expression of tau [10].

97

98 Using our system, which relies on physiological neuronal uptake of tau aggregates supplied  
99 to the media, we show that neurons within CA1 are preferentially susceptible to seeded  
100 aggregation, displaying intracellular hyperphosphorylated tau tangles. We find that seeding  
101 activity cannot be titrated down and only occurs at high concentrations of tau assemblies.  
102 Crucially, at between 30 and 100 nM, the concentrations of tau assemblies required to initiate  
103 seeding exceed reported measures of physiological ISF and CSF tau. Our results imply that  
104 a model of tau spread via seeded aggregation requires these concentrations to be locally  
105 exceeded or requires other mechanisms not captured here to facilitate seeded aggregation.

106

107

108

109

## 110 **Results**

111 Sagittal hippocampal slices of ~300  $\mu\text{m}$  thickness were prepared from homozygous P301S  
112 tau-transgenic mice at age 7 d. Hippocampal structures are well developed at this age, yet the  
113 tissue exhibits plasticity that aids recovery from the slicing procedure [23]. We stained OHSCs  
114 with antibodies against markers of the major cell types of the brain: neurons (Map2), microglia  
115 (Iba1) and astrocytes (Gfap) [Figure 1a]. Similar to previous studies [19], neurons were found  
116 to maintain extensive arborisation with evidence of intact neuronal tracts. Microglia were  
117 observed with normal morphology with extensive processes, similar to quiescent cells in whole  
118 brains [24]. Astrocytes were also well represented throughout the cultures. Immunostaining  
119 for tau revealed widespread expression in all regions of the hippocampus [Figure 1b]. After 5  
120 weeks in culture no overt signs of tau pathology were apparent, as visualised by staining with  
121 AT8 [Figure 1c]. These results demonstrate that hippocampal architecture and cell types from  
122 P301S tau transgenic mice are maintained through the slicing and culture process.  
123 Importantly, they demonstrate that OHSCs from P301S tau transgenic mice do not undergo  
124 detectable spontaneous aggregation over this time period.

125  
126 To investigate the response of slice cultures to challenge with tau assemblies, we prepared  
127 tau from two independent sources. First, we expressed the 0N4R isoform of tau bearing the  
128 P301S mutation in *E. coli*. Recombinant protein was incubated with heparin and, following a  
129 lag period, was found to give a fluorescence signal in the presence of thioflavin T, a dye whose  
130 fluorescence increases upon binding to  $\beta$ -sheet rich amyloid structures [Figure 2a]. Negative  
131 stain transmission electron microscopy revealed the presence of abundant filamentous  
132 structures [Figure 2b]. Second, we prepared the sarkosyl-insoluble (SI) fraction from aged  
133 P301S tau transgenic mice, a procedure that enriches insoluble tau species. Brain-derived  
134 assemblies were subjected to western blot, confirming the presence of hyperphosphorylated,  
135 insoluble tau [Figure 2c]. The samples were quantified using a dot-blot method using  
136 recombinant fibrillar tau as a standard [Supplementary Figure 1]. Tau assemblies were added  
137 to HEK293 cells stably expressing 0N4R P301S tau-venus, a reporter cell line for seeded  
138 aggregation [25]. In this assay, transfection reagents are used to deliver tau assemblies into

139 cells, whereupon tau-venus is observed to form puncta over 1-2 d. This aggregation was  
140 previously found to result in the accumulation of tau-venus in the sarkosyl-insoluble pellet [25].  
141 In the present study, abundant venus-positive puncta were detected following challenge with  
142 recombinant fibrils or mouse brain derived tau [Figure 2d]. To investigate whether these  
143 seeded assemblies bore markers of tau hyperphosphorylation, we stained with the  
144 monoclonal antibody AT8 and AT100, which recognises tau phosphorylated at pT212 and  
145 pS214. These epitopes occur on tau filaments extracted from post-mortem tauopathy brains  
146 including those from Alzheimer's disease patients. We observed that challenge with  
147 recombinant tau assemblies resulted in colocalization between tau-venus puncta and AT8 or  
148 AT100 [Figure 2e,f]. We therefore concluded that our tau preparations contained species able  
149 to induce *bona fide* seeded aggregation in recipient cells.

150

151 Next, we challenged OHSCs with tau assemblies. Recombinant or mouse brain-derived tau  
152 assemblies were supplied to the culture media for a period of three days followed by twice-  
153 weekly media changes [Figure 3a]. Three weeks after challenge with 100 nM recombinant tau  
154 assemblies or 5  $\mu$ l SI tau we observed pronounced AT8 staining [Figure 3b][Supplementary  
155 Figure 1], suggesting the presence of mature hyperphosphorylated tau assemblies. The  
156 addition of monomeric tau did not induce these same structures, indicating that the misfolded  
157 state of tau was responsible for seeded aggregation [Figure 3b]. Furthermore, addition of tau  
158 assemblies to OHSCs prepared from wildtype mice did not induce seeded aggregation  
159 suggesting that the transgenic P301S tau construct is responsible for the phenotype [Figure  
160 3b]. The levels of AT8 between unseeded WT and P301S OHSCs were non-significant [Figure  
161 3c]. We also observed the accumulation of sarkosyl-insoluble species following seeding in  
162 P301S transgenic OHSC but not wildtype OHSCs [Figure 3d,e][Supplementary Figure 2].  
163 Taken together, these data demonstrate that insoluble, hyperphosphorylated tau assemblies  
164 can be induced in transgenic OHSCs by the addition of exogenous tau assemblies.

165

166 To further characterise the induced aggregates, we investigated the subcellular and regional  
167 location of tau lesions. We used recombinant tau assemblies to induce seeding owing to the  
168 high confidence that AT8-reactive aggregates result from seeded aggregation rather than the  
169 input tau. Within cell bodies, we observed large aggregates in peri-nuclear regions [Figure  
170 4a]. Additionally, numerous smaller tau puncta were found along the length of neurites. Puncta  
171 were interrupted by regions apparently devoid of hyperphosphorylated tau. In contrast, Map2  
172 staining revealed the presence of intact neurites, indicating that the punctate distribution of  
173 tau is not a consequence of neuronal fragmentation. They further demonstrate that neurons  
174 are able to tolerate tau aggregation to a certain degree without gross loss of morphology or  
175 overt toxicity. We compared levels of seeding between regions of the hippocampal slices. We  
176 observed the presence of AT8 positive structures in neurons within all subdivisions [Figure  
177 4b]. However, AT8 reactivity was considerably greater within the CA1 region compared to CA2  
178 and CA3. Approximately 80% of AT8-positive structures were found in CA1, compared to  
179 ~10% in each of CA2 and CA3 [Figure 4c]. We examined levels of tau as a potential underlying  
180 cause of CA1 susceptibility but observed comparable expression levels across different  
181 regions [Figure 4d]. In summary, these results demonstrate that challenge of OHSCs with  
182 assemblies of tau induces the accumulation of pathology in neurites and cell bodies,  
183 predominantly in CA1 neurons, resulting in widespread accumulation of intracellular  
184 hyperphosphorylated tau structures.

185

186 To determine the time-dependence of this tau pathology, we next performed a time course  
187 following the addition of seed. Slices were fixed at 1, 2 or 3 weeks following challenge with  
188 100 nM recombinant assemblies [Figure 5a]. Alternatively, slice cultures were fixed at 3 weeks  
189 following challenge with buffer only. As above, slices that were not exposed to tau assemblies  
190 developed no robust evidence of hyperphosphorylated tau puncta. However, challenge with  
191 tau assemblies resulted in increasing levels of bright AT8-positive structures over time,  
192 consistent with seeded aggregation of intracellular pools of tau [Figure 5b]. At 1 week after  
193 challenge, isolated AT8 positive puncta were observed as well as diffuse AT8 staining. A week

194 later, puncta became more numerous and a few large aggregates were observed. However,  
195 3 weeks after challenge with tau assemblies, AT8 staining was widespread with the presence  
196 of numerous aggregates that occupied entire cell bodies. The increase in AT8 staining  
197 followed an exponential curve with a doubling time of ~7 days. The size of AT8-positive  
198 structures was similarly found to increase over time. Stained areas greater than 50  $\mu\text{m}^2$ ,  
199 generally only present within cell bodies, were found to be largely absent at 1 week post-  
200 challenge but subsequently to increase in prevalence [Figure 5d]. This suggests that  
201 amplification of aggregates within individual neurons is driving the overall increase in AT8  
202 signal. The results are therefore consistent with a model of growth of hyperphosphorylated tau  
203 structures via a process of templated aggregation following exposure to seed-competent tau  
204 assemblies.

205

206 The above results demonstrate that our OHSC model exhibits behaviour consistent with prion-  
207 like spread of tau. However, the dose we used (100 nM monomer equivalent) represents a  
208 concentration in excess of ISF and CSF tau concentrations, which occupy the low nanomolar  
209 to picomolar region. We therefore investigated the response of OHSCs to varying of the dose  
210 of exogenously-supplied tau assemblies. Remarkably, we found that a reduction of seed  
211 concentration from 100 nM to 30 nM resulted in virtually no seeded aggregation being  
212 detectable within the slice [Figure 6a]. Whereas cell bodies reactive for AT8 could be observed  
213 when challenged with 100 nM tau assemblies, only very rare and small AT8-positive  
214 assemblies in neurites were observed following challenge with 30 nM tau. Conversely,  
215 increasing exogenous tau concentration from 100 nM to 300 nM increased the AT8-  
216 immunoreactive area by almost 10-fold [Figure 6b]. To exclude any effect of the culture  
217 membrane on the efficiency of tau uptake, we applied tau at the same concentrations directly  
218 to the surface of the slices. We challenged OHSCs with 25  $\mu\text{l}$  of recombinant tau aggregates  
219 applied to the apical surface of the slice. Alternatively, we supplied the same concentration of  
220 tau assemblies to the media as normal. Under both experimental set-ups we observed robust  
221 induction of seeding at 100 nM, but not at 30 nM [Figure 6c]. Thus, the local concentration of

222 tau governs seeded aggregation and is independent of application route. These results  
223 demonstrate that tau seeding in OHSCs only occurs efficiently at concentrations above 100  
224 nM of supplied assemblies.

225

226 Independently acting infectious particles such as viruses retain infectivity upon dilution until  
227 they are diluted out at endpoint. They display one-hit dynamics where proportion of infected  
228 cells,  $P(I)$ , can be described by the equation  $P(I) = 1 - e^{-m}$  where  $m$  is the average number of  
229 infectious agents added per cell. To determine whether tau assemblies display these  
230 properties, we titrated tau assemblies on HEK293's expressing tau-venus. Here, where  
231 conditions have been optimised for sensitive detection of seeding, and tau assemblies are  
232 delivered directly to the cytoplasm with transfection reagents, we observe that seeding activity  
233 is proportional to dose and can be titrated down. The observed level of seeding approximates  
234 a one-hit titration curve [Figure 7a]. Thus, tau assemblies have the intrinsic ability to act as  
235 independent particles when tested in reporter cell lines. This is in direct contrast to the results  
236 observed in OHSCs where seeding reduces much more rapidly as tau assemblies are diluted  
237 than would be expected under a single-hit model [Figure 7a]. One potential explanation for  
238 these differences is that clearance mechanisms in intact tissue inherently prevent single-  
239 particle activity. To test this, we titrated AAV1/2.hSyn-GFP particles expressing GFP and  
240 measured the percent of Map2-positive neurons that were transduced. We observed that  
241 AAV1/2 behaved in a manner consistent with one-hit dynamics [Figure 7b]. Thus, tau  
242 assemblies differ from classical infectious agents and do not titrate in a manner expected of  
243 independently acting particles in mouse neural tissue. Rather, seeding is a behaviour that only  
244 emerges at high concentrations of extracellular tau assemblies.

245

246 **Discussion**

247

248 Elucidating the mechanism of tau aggregation and its apparent spread through the brain is  
249 critical to the development of mechanism-based therapeutics. The ‘prion-like’ model of tau  
250 spread posits that the transit of assembled tau species from affected to naïve cells promotes  
251 the exponential spread of pathological tau over time and space within a diseased brain. In  
252 support of this model, extracellular fluids of tauopathy patients’ brains contain seed-competent  
253 tau species: CSF samples from both AD and Pick’s disease patients give rise to seeded  
254 aggregation in biosensor cell lines and biochemical detection assays [26–28]. Further  
255 evidence in support of the prion-like model comes from *in vivo* challenge experiments:  
256 intracranial injection of assembled tau can result in induced tau pathology in wildtype or tau-  
257 transgenic rodent brains. Understanding how these *in vivo* challenge experiments, which are  
258 typically performed at high concentration [Figure 7c, Supplementary Table 1], translate to  
259 physiological concentrations is important in order to assess the applicability of these results  
260 to disease mechanisms. Contrary to our expectations, we found that tau seeding activity  
261 rapidly dropped away upon dilution in OHSCs. Observations of seeding behaviour at high  
262 concentration therefore cannot necessarily be extrapolated down to inform on the behaviour  
263 of tau at lower concentrations.

264

265 In reporter cells, we observed that tau seeds titrated in a one-hit manner, as expected of  
266 independently acting particles. This suggests that reporter cell lines which have been validated  
267 in this way can be used to ascertain the intrinsic seeding activity of tau preparations, which  
268 can then be expressed as seeding units per quantity tau, analogous to other infectious agents.  
269 In OHSCs, tau seeding was observed at concentrations in excess of 100 nM. Further dilution  
270 of tau assemblies prevented seeded aggregation long before end-point dilution of seeds  
271 therefore displaying a marked deviation from one-hit dynamics. Such deviations in virus  
272 infectivity can be caused by host cell factors that prevent infection becoming saturated by high  
273 viral dose [29,30]. By analogy, we consider it likely that homeostatic mechanisms act to  
274 prevent seeded aggregation of tau but become saturated by high tau concentrations. The

275 nature of any such saturable barrier to seeding is not clear. One possibility is that phagocytic  
276 cells present in slices preclude observations of one-hit dynamics. This was not the case,  
277 however, since AAV particles were found to titrate with one-hit dynamics in OHSCs. A trivial  
278 explanation of tau at low concentration being unable to cross the membrane was also ruled  
279 out. Other mechanisms are therefore implicated such as saturation of proteostatic  
280 mechanisms or uptake to the cell. Identification of these defences may provide a valuable  
281 route to understanding the mechanisms which prevent prion-like propagation, and their  
282 potential deterioration in disease.

283

284 Our results suggest that healthy neural tissue is able to withstand the concentration of tau  
285 present in extracellular fluids without observable seeded aggregation. The effective threshold  
286 for seeding, measured here at around 100 nM, exceeds physiological ISF/CSF concentrations  
287 by several orders of magnitude. Thus, in order for spreading via seeded aggregation to occur,  
288 our results suggest that other mechanisms are required. For instance, uncontrolled neuronal  
289 cell death or release of tau into synaptic clefts may transiently raise the local concentration of  
290 tau to high levels. Alternatively, the threshold for seeded tau aggregation may be altered in  
291 the degenerating brain, for instance through inflammation or other mechanisms. Finally, other  
292 modes of transmission within the brain that do not rely on naked pools of extracellular tau may  
293 circumvent the non-linear dose response observed here. Such mechanisms include tau  
294 spreading via tunnelling nanotubules and in extracellular vesicles [31,32].

295

296 The tau species present in the extracellular spaces of the brain are likely to differ from those  
297 used here in terms of pathological fold, post-translational modification and proteolytic  
298 truncation. Potentially of interest in this regard is the study by Skachokova and colleagues  
299 who successfully induced seeding following injection of P301S tau transgenic mice with a  
300 1,000-fold concentrate of CSF from AD patients [33]. At 5-17 nM, these samples are still far  
301 in excess of human CSF tau concentrations. But, notably, these concentrations are below the  
302 threshold defined in our OHSCs model [Figure 7c]. Future work is therefore required to



303 determine whether mechanisms not captured here but present within the degenerating brain  
304 enable seeded aggregation to occur. Future studies should therefore seek to develop seeding  
305 in wildtype, preferably human, settings in order to assess the nature of seeding of human  
306 brain-origin tau assemblies.

307

308 Our experiments demonstrated that neurons in CA1 were particularly sensitive to seeded  
309 aggregation compared to those in CA2 and CA3. Whilst injection of tau assemblies to the *in*  
310 *vivo* brain also demonstrates prominent CA1 seeding, proximity to the injection site is the  
311 major determinant of seeding in animal studies, thereby confounding conclusions of regional  
312 susceptibility [3,5,34]. We found that tau substrate levels were not implicated in the phenotype,  
313 suggesting that other factors are responsible for the increased susceptibility. These results  
314 are potentially of interest in the study of selective vulnerability since it is well established that  
315 CA1 displays more pronounced AT8 reactivity in post-mortem human brains [8,35,36]. In  
316 humans, the advanced pathology in CA1 versus other HC regions could potentially be  
317 explained either by selective vulnerability of its neurons to aggregation, or by its upstream  
318 position in the circuitry of the HC and therefore prone to earlier and more pronounced  
319 pathology under a spreading model. Our findings lend support to an underlying increased  
320 susceptibility of CA1 neurons to pathology. OHSCs therefore provide a suitable platform for  
321 future studies to determine the biological basis of this susceptibility.

322

323 Our findings help define the prion-like characteristics of tau assemblies. Whilst intrinsic  
324 seeding activity that titrates according to one-hit dose-response can be detected in biosensor  
325 assays, this behaviour is lost in neural tissue. Our findings suggest that neural tissue  
326 possesses homeostatic mechanisms that are capable of successfully preventing seeded  
327 aggregation. Saturating levels of tau assemblies are required to overcome these barriers to  
328 initiate seeded aggregation.

329

## 330 **Materials and Methods**

### 331 **Mouse lines**

332 All animal work was licensed under the UK Animals (Scientific Procedures) Act 1986 and  
333 approved by the Medical Research Council Animal Welfare and Ethical Review Body. P301S  
334 tau transgenic mice [21] that had been extensively backcrossed to C57BL/6 background were  
335 obtained from Dr Michel Goedert, MRC Laboratory of Molecular Biology, UK. Male and female  
336 were used in the study and humanely sacrificed by cervical dislocation.

### 337 **Recombinant tau production**

338 The expression and purification of recombinant human 0N4R tau bearing the P301S mutation  
339 from *E. coli* BL-21 (DE3, Agilent Technologies) was performed as described previously  
340 (Goedert and Jakes, 1990) with small modifications. Bacterial pellets were collected through  
341 centrifugation (3300 g, 4 °C, 10 min) and then resuspended in 10 ml/l of culture with buffer A  
342 (50 mM MES pH 6.5, 10 mM EDTA, 14 mM  $\beta$ -mercaptoethanol, 0.1 mM PMSF, 1 mM  
343 benzamidine, 1x complete EDTA-free protease inhibitors). The resuspended bacteria were  
344 lysed on ice using a probe sonicator (approximately 60% amplitude) and then boiled for 10  
345 min at 95 °C to pellet the majority of proteins, while tau will remain in solution as a natively  
346 unfolded protein. Denatured proteins were pelleted through ultracentrifugation (100,000 g, 4  
347 °C, 50 min). The clarified supernatant containing monomeric tau P301S was then passed  
348 through a HiTrap CantoS (Cytiva) cation exchange column and the bound proteins were eluted  
349 through a 0-50 % gradient elution with Buffer A containing 1 M NaCl. Eluted fractions were  
350 assessed through SDS-PAGE and total protein staining with Coomassie InstantBlue.  
351 Fractions of interest were concentrated using 10 kDa cut-off Amicon Ultra-4 concentrators  
352 (Merck Millipore) before loading on a Superdex 200 10/300 GL (Cytiva) size exclusion  
353 chromatography column. The final tau P301S protein was stored in PBS containing 1 mM  
354 DTT. All the affinity purification and size exclusion chromatography steps were performed  
355 using the ÄKTA Pure system (Cytiva).

### 356 **Recombinant Tau Aggregation**

357 Tau monomer was added to aggregation buffer (20  $\mu$ M Heparin, 60  $\mu$ M P301S tau monomer,  
358 1x complete EDTA-free protease inhibitors, 2  $\mu$ M DTT in PBS) and incubated at 37 °C for 3  
359 days. The resulting P301S tau filaments were sonicated for 15 seconds before long-term  
360 storage at -80 °C.

### 361 **ThioflavinT Assay**

362 Tau monomer was added to aggregation buffer, with 10  $\mu$ M sterile filtered ThioflavinT (ThT).  
363 Samples were loaded in triplicate into black 96-well plates. Plates were loaded into a  
364 CLARIOstar (BMG Labtech), and measurements were taken every 5 minutes after shaking,  
365 for 72 hours at 37 °C min (excitation and emission wavelength 440 nm and 510 nm  
366 respectively).

### 367 **TEM**

368 Recombinant tau fibrils were mounted on carbon-coated copper grids (EM Resolutions) via  
369 suspension of the grid on a single droplet. The grid was then stained with 1% uranyl acetate  
370 and imaged with a FEI Tecnai G20 electron microscope operating at 200kV and an AMT  
371 camera.

### 372 **Preparation of tau assemblies from brains and OHSCs**

373 Tau was extracted from aged brains (26 weeks) from mice transgenic for human P301S tau  
374 using sarkosyl extraction. Tissues were homogenised for 30 s in 4 volumes of ice-cold H-  
375 Buffer (10mM Tris pH 7.4, 1mM EGTA, 0.8M NaCl, 10% sucrose, protease and phosphatase  
376 inhibitors (Halt™ Protease and Phosphatase Inhibitor Cocktail)) using the VelociRuptor V2  
377 Microtube Homogeniser (Scientific Laboratory Supplies). The homogenates were spun for 20  
378 minutes at 20,000  $\times$  g and supernatant was collected. The resulting pellet was re-  
379 homogenised as above in 2 volumes of ice-cold H-Buffer and processed as above.  
380 Supernatants from both spins were combined and sarkosyl was added to a final concentration  
381 of 1% and incubated for 1 h at 37 °C. Supernatants were then spun at 100,000  $\times$  g at 4 °C for  
382 1 h. The resulting pellet was resuspended in 0.2 volumes of PBS and sonicated for 15 s in a  
383 water-bath sonicator before storage at -80 °C. For OHSCs, the same procedure was followed,

384 except slices were freeze thawed 5 times in 20  $\mu$ l per slice ice-cold H-Buffer and the final pellet  
385 was resuspended in 5  $\mu$ l per slice PBS.

### 386 **Western blotting**

387 Samples were transferred to fresh microcentrifuge tubes, to which appropriate volumes of 4 $\times$   
388 NuPAGE LDS sample buffer (Thermo Fisher) containing 50 mM DTT was added and heated  
389 to 95 °C for 5 min. Samples were resolved using NuPAGE Bis–Tris Novex 4–12% gels (Life  
390 Technologies) and electroblotted to a 0.2- $\mu$ m PVDF membrane using the Transblot Turbo  
391 Transfer System (Bio-Rad). Membranes were blocked with 5% milk TBS–Tween 20 before  
392 incubation with primary antibodies overnight at 4 °C. Membranes were then probed with  
393 appropriate secondary antibodies conjugated with HRP for 1 h. Membranes were washed  
394 repeatedly in TBS–0.1% Tween-20 after both primary and secondary antibody incubation.  
395 Blots were incubated with Pierce Super Signal or Millipore Immobilon enhanced  
396 chemiluminescence reagents for 5 min and visualised using a ChemiDoc system (Bio-Rad).

397

### 398 **Dot Blot**

399 Recombinant or mouse-extracted tau fibrils were diluted in PBS as indicated in Supplementary  
400 Figure 1 and applied to 0.2  $\mu$ m nitrocellulose membrane using the Bio-Dot microfiltration  
401 apparatus (Bio-Rad). The membranes were then blocked in 5% milk TBS-Tween 20 and  
402 subsequently incubated with primary antibody overnight. The next day, the membranes were  
403 probed with appropriate secondary antibodies conjugated with Alexa488 fluorophore and  
404 imaged using the ChemiDoc system (Bio-Rad). The dot intensities were quantified with the  
405 Image Studio Lite software (LI-COR Biosciences) and the values for the recombinant fibrils  
406 were fitted to a simple linear regression curve.

### 407 **Seeding assay in HEK293**

408 The seeding assay was carried out as described previously [25]. Briefly, HEK293 P301S tau-  
409 venus cells were plated at 15,000 cells per well in black 96-well plates pre-coated with poly  
410 D-lysine in 50  $\mu$ l OptiMEM (Thermo Fisher). Tau assemblies were diluted in 50  $\mu$ l OptiMEM  
411 (Thermo Fisher) and added to cells with 0.5  $\mu$ l per well Lipofectamine 2000. After 1.5 h, 100

412  $\mu$ L complete DMEM was added to each well to stop the transfection process. Cells were  
413 incubated at 37 °C in an IncuCyte® S3 Live-Cell Analysis System for 48 - 72 h after addition  
414 of fibrils.

#### 415 **Preparation and culturing of organotypic slices**

416 Organotypic hippocampal slice cultures were prepared and cultured according to the protocols  
417 described previously [19,23]. Brains from P6-P9 pups were rapidly removed and kept in ice-  
418 cold Slicing medium (EBSS + 25 mM HEPES+ 1x Penicillin/Streptomycin) on ice. All  
419 equipment was kept ice-cold. Brains were bisected along the midline and the cerebellum was  
420 removed using a sterile scalpel. The medial, cut surface of the brain was adhered to the stage  
421 of a Leica VT1200S Vibratome using cyanoacrylate (Loctite Super Glue) and the vibratome  
422 stage was flooded with ice-cold Slicing medium. Hemispheres were arranged such that the  
423 vibratome blade sliced in a rostral to caudal direction. Sagittal slices of 300  $\mu$ m thickness were  
424 prepared and the hippocampus was sub-dissected using sterile needles. Hippocampal slices  
425 were transferred to 15 mL tubes filled with ice-cold Slicing medium using sterile plastic pipettes  
426 with the ends cut off. Slices were then transferred onto sterile 0.4  $\mu$ m pore membranes  
427 (Millipore PICM0RG50) in 6-well plates pre-filled with 1 mL pre-warmed Culture medium (50%  
428 MEM with GlutaMAX, 18% EBSS, 6% EBSS+D-Glucose, 1% Penicillin-Streptomycin, 0.06%  
429 nystatin and 25% Horse Serum) and incubated at 37 °C in a humid atmosphere with 5% CO<sub>2</sub>.  
430 Three slices were typically maintained per well. 24 h after plating 100% media was exchanged  
431 and thereafter a 50% media exchange was carried out twice per week. For seeding  
432 experiments, tau assemblies were diluted in Culture medium and added to the underside of  
433 the membrane with 100% media change. After three days, assemblies were removed by 100%  
434 media change.

#### 435 **Adeno-associated virus**

436 AAV1/2.hSyn-GFP particles were generated by co-transfection of HEK293T cells with AAV2/1  
437 (Addgene 112862), AAV2/2 (Addgene 104963), adenovirus helper plasmid pAdDeltaF6  
438 (Addgene 112867) and pAAV-hSyn-EGFP (Addgene 50465). Virus particles were purified by  
439 iodixanol gradient in at T70i ultracentrifuge rotor as previous [37]. Viral purity was confirmed

440 by the presence of three bands following SDS-PAGE and staining with Coomassie  
441 InstantBlue.

#### 442 **Immunofluorescence microscopy**

443 Slices on membranes were washed with PBS and then fixed in 4% (w/v) paraformaldehyde  
444 for 20 min at 37 °C. Subsequently, membranes were rinsed 2–3 times with PBS and left  
445 shaking gently for 15 min to remove traces of paraformaldehyde before subsequent  
446 processing. Slices were permeabilised with 0.5% (v/v) Triton X-100 in immunofluorescence  
447 blocking buffer (IF block) (3% goat serum in 1× PBS) for 1 h at room temperature, and rinsed  
448 with 3x with TBS. Slices were then incubated with primary antibodies diluted in IF block  
449 overnight at 4 °C, rinsed with 3 times with TBS, and incubated for 2 h in the dark with  
450 secondary antibodies, also diluted in IF block. Secondary antibodies conjugated to Alexa  
451 Fluor 488, 568 or 647 were obtained from Thermo Fisher. Following rinsing 3x with TBS, the  
452 slices were incubated with Hoechst stain for 10 min and rinsed 3x with TBS. Membranes were  
453 placed on slides (slice side up), mounting medium (ProLong Diamond, Life Technologies) was  
454 added and a cover slip was placed on top of the slice. Images were captured using a Zeiss  
455 LSM780 Confocal Microscope with either a 20x or a 63x objective lens. Images were collected  
456 and stitched, where appropriate, using ZEISS Zen software package.

#### 457 **Image Analysis and statistics**

458 For tau seeding assays in HEK293 cells, aggregates were detected and quantified using the  
459 ComDet plugin in Fiji [38]. Threshold levels for detection of aggregates were adjusted using  
460 mock-seeded images for each experiment. Levels of seeding were calculated as (number of  
461 aggregates)/(total cells) × 100 for individual fields. For slice cultures, maximum intensity Z-  
462 projections were interrogated for AT8 immunoreactivity by the application of a binary  
463 threshold-based mask in ImageJ. Percent area of AT8 reactivity was determined in regions of  
464 100 x 100 μm. GFP positive neurons upon AAV infection were analysed in the same way. For  
465 measures of number of neurons affected in hippocampal subregions, a manual count of cell  
466 bodies positive for AT8 immunoreactivity was performed. Zero values were given an arbitrary  
467 value of 10<sup>-5</sup> for representation on log-scale axes. The data in all graphs are represented as

468 the mean +/- SD. Data was analysed via the Kruskal-Wallis test by ranks, unless it was  
469 determined to be normally distributed, in which case a one-way ANOVA was employed. All  
470 statistics were carried out in GraphPad Prism Version 8.

471

472 **Acknowledgments**

473 We thank Dr Michel Goedert for provision of P301S tau transgenic mice and Cambridge  
474 Advanced Imaging Centre for access to electron microscope facilities. We thank Prof Sir David  
475 Klenerman for valuable discussions on the early versions of this manuscript.

476 **Funding**

477 WAM is supported by a Sir Henry Dale Fellowship jointly funded by the Wellcome Trust and  
478 the Royal Society (Grant Number 206248/Z/17/Z). This work was supported by the UK  
479 Dementia Research Institute which receives its funding from DRI Ltd, funded by the UK  
480 Medical Research Council, Alzheimer's Society and Alzheimer's Research UK. This project  
481 has received funding from the Innovative Medicines Initiative 2 Joint Undertaking under grant  
482 agreement No 116060 (IMPRiND). This Joint Undertaking receives support from the European  
483 Union's Horizon 2020 research and innovation programme and EFPIA. This work is supported  
484 by the Swiss State Secretariat for Education, Research and Innovation (SERI) under contract  
485 number 17.00038. The work also received funding from Takeda Pharmaceuticals Company.  
486 LVCM is supported by the UK Medical Research Council.

487

488 **Author contributions**

489 Conceived research: WAM, MPC, ASM, LVCM; Designed experiments: ASM, LVCM, WAM;  
490 Developed slice culture assay: ASM, LVCM, CD, OS, CK, MJV, LCJ; Performed experiments  
491 and analysed data: ASM, LVCM, TK, BJT, WAM, SS, SC. All authors contributed to writing  
492 and editing of the manuscript.

493 **Competing interests**

494 The authors declare that they have no competing interests.

495 **Ethics Approval**



496 All animal work was licensed under the UK Animals (Scientific Procedures) Act 1986 and  
497 approved by the Medical Research Council Animal Welfare and Ethical Review Body.

498

499

500

501 **References**

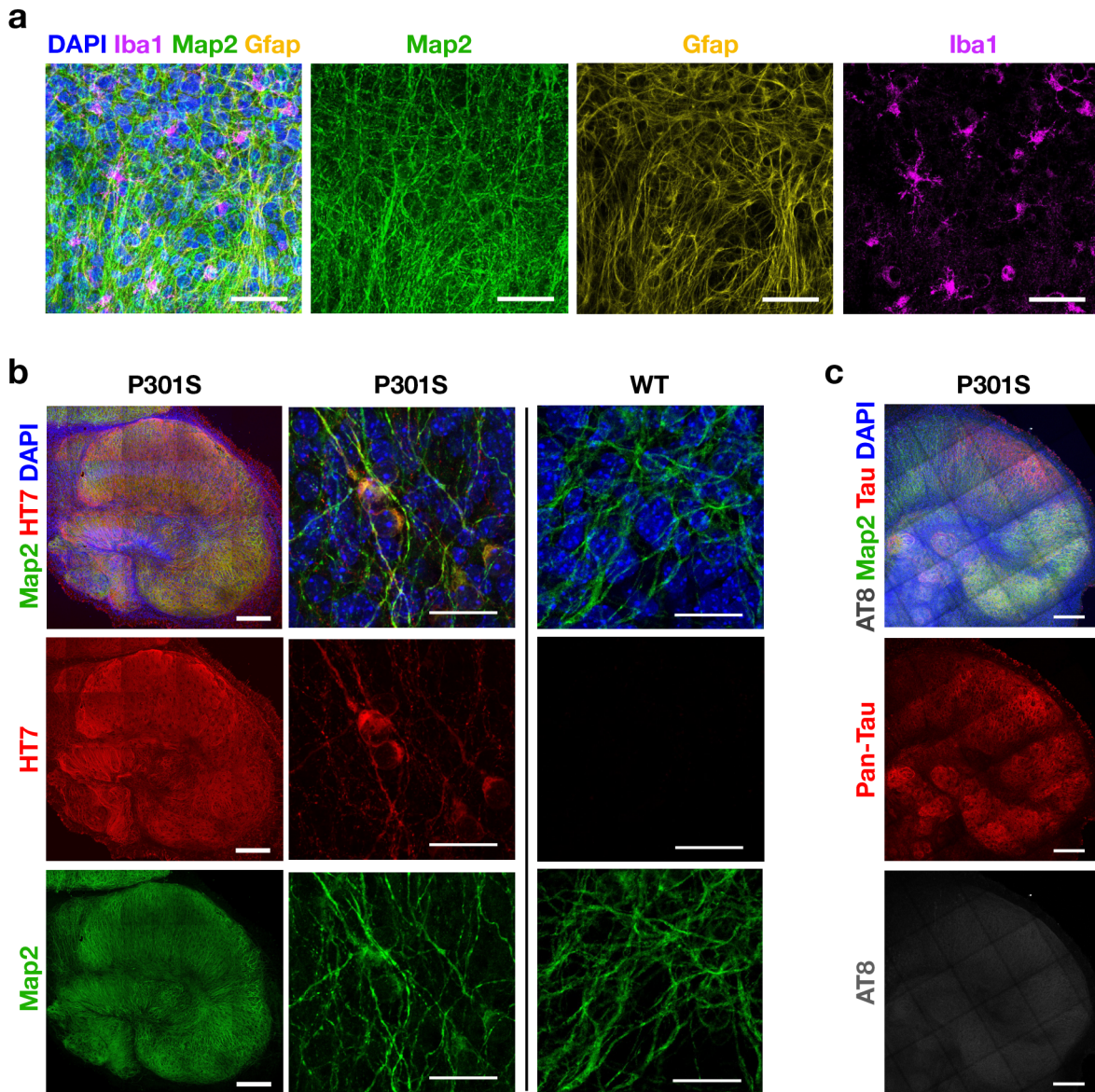
- 502 1. Goedert M. Alzheimer's and Parkinson's diseases: The prion concept in relation to  
503 assembled A $\beta$ , tau, and  $\alpha$ -synuclein. *Science*. 2015;349:1255555.
- 504 2. Jucker M, Walker LC. Propagation and spread of pathogenic protein assemblies in  
505 neurodegenerative diseases. *Nat Neurosci*. 2018;21:1341–9.
- 506 3. Clavaguera F, Bolmont T, Crowther RA, Abramowski D, Frank S, Probst A, et al.  
507 Transmission and spreading of tauopathy in transgenic mouse brain. *Nat Cell Biol*.  
508 2009;11:909–13.
- 509 4. Frost B, Jacks RL, Diamond MI. Propagation of tau misfolding from the outside to the inside  
510 of a cell. *J Biol Chem*. 2009;284:12845–52.
- 511 5. Iba M, Guo JL, McBride JD, Zhang B, Trojanowski JQ, Lee VM-Y. Synthetic Tau Fibrils  
512 Mediate Transmission of Neurofibrillary Tangles in a Transgenic Mouse Model of  
513 Alzheimer's-Like Tauopathy. *J Neurosci*. Society for Neuroscience; 2013;33:1024.
- 514 6. Goedert M, Jakes R, Vanmechelen E. Monoclonal antibody AT8 recognises tau protein  
515 phosphorylated at both serine 202 and threonine 205. *Neurosci Lett*. 1995;189:167–  
516 70.
- 517 7. Braak H, Thal DR, Ghebremedhin E, Del Tredici K. Stages of the Pathologic Process in  
518 Alzheimer Disease: Age Categories From 1 to 100 Years. *J Neuropathol Exp Neurol*.  
519 Oxford Academic; 2011;70:960–9.
- 520 8. Braak H, Braak E. Neuropathological staging of Alzheimer-related changes. *Acta*  
521 *Neuropathol (Berl)*. 1991;82:239–59.
- 522 9. Nelson PT, Alafuzoff I, Bigio EH, Bouras C, Braak H, Cairns NJ, et al. Correlation of  
523 Alzheimer Disease Neuropathologic Changes With Cognitive Status: A Review of the  
524 Literature. *J Neuropathol Exp Neurol*. 2012;71:362–81.
- 525 10. Yamada K, Cirrito JR, Stewart FR, Jiang H, Finn MB, Holmes BB, et al. In Vivo  
526 Microdialysis Reveals Age-Dependent Decrease of Brain Interstitial Fluid Tau Levels  
527 in P301S Human Tau Transgenic Mice. *J Neurosci*. 2011;31:13110–7.

- 528 11. Sjögren M, Vanderstichele H, Agren H, Zachrisson O, Edsbacke M, Wikkelsø C, et al. Tau  
529 and Abeta42 in cerebrospinal fluid from healthy adults 21-93 years of age:  
530 establishment of reference values. *Clin Chem*. 2001;47:1776–81.
- 531 12. Blennow K. A Review of Fluid Biomarkers for Alzheimer’s Disease: Moving from CSF to  
532 Blood. *Neurol Ther*. 2017;6:15–24.
- 533 13. Dulbecco R, Vogt M. Some problems of animal virology as studied by the plaque  
534 technique. *Cold Spring Harb Symp Quant Biol*. 1953;18:273–9.
- 535 14. Masel J, Jansen VAA. The measured level of prion infectivity varies in a predictable way  
536 according to the aggregation state of the infectious agent. *Biochim Biophys Acta BBA*  
537 - *Mol Basis Dis*. 2001;1535:164–73.
- 538 15. Dunwiddie T, Lynch G. Long-term potentiation and depression of synaptic responses in  
539 the rat hippocampus: localization and frequency dependency. *J Physiol*.  
540 1978;276:353–67.
- 541 16. Cho S, Wood A, Bowlby MR. Brain Slices as Models for Neurodegenerative Disease and  
542 Screening Platforms to Identify Novel Therapeutics. *Curr Neuropharmacol*. 2007;5:19–  
543 33.
- 544 17. Croft CL, Futch HS, Moore BD, Golde TE. Organotypic brain slice cultures to model  
545 neurodegenerative proteinopathies. *Mol Neurodegener*. 2019;14:45.
- 546 18. Duff K, Noble W, Gaynor K, Matsuoka Y. Organotypic slice cultures from transgenic mice  
547 as disease model systems. *J Mol Neurosci*. 2002;19:317–20.
- 548 19. Harwell CS, Coleman MP. Synaptophysin depletion and intraneuronal A $\beta$  in organotypic  
549 hippocampal slice cultures from huAPP transgenic mice. *Mol Neurodegener*.  
550 2016;11:44.
- 551 20. Croft CL, Wade MA, Kurbatskaya K, Mastrandreas P, Hughes MM, Phillips EC, et al.  
552 Membrane association and release of wild-type and pathological tau from organotypic  
553 brain slice cultures. *Cell Death Dis*. 2017;8:e2671.

- 554 21. Allen B, Ingram E, Takao M, Smith MJ, Jakes R, Virdee K, et al. Abundant tau filaments  
555 and nonapoptotic neurodegeneration in transgenic mice expressing human P301S tau  
556 protein. *J Neurosci Off J Soc Neurosci*. 2002;22:9340–51.
- 557 22. Kundel F, Hong L, Falcon B, McEwan WA, Michaels TCT, Meisl G, et al. Measurement of  
558 Tau Filament Fragmentation Provides Insights into Prion-like Spreading. *ACS Chem*  
559 *Neurosci*. 2018;9:1276–82.
- 560 23. De Simoni A, MY Yu L. Preparation of organotypic hippocampal slice cultures: interface  
561 method. *Nat Protoc*. Nature Publishing Group; 2006;1:1439–45.
- 562 24. Sheppard O, Coleman MP, Durrant CS. Lipopolysaccharide-induced neuroinflammation  
563 induces presynaptic disruption through a direct action on brain tissue involving  
564 microglia-derived interleukin 1 beta. *J Neuroinflammation*. 2019;16:106.
- 565 25. McEwan WA, Falcon B, Vaysburd M, Clift D, Oblak AL, Ghetti B, et al. Cytosolic Fc  
566 receptor TRIM21 inhibits seeded tau aggregation. *Proc Natl Acad Sci U S A*.  
567 2017;114:574–9.
- 568 26. Takeda S, Commins C, DeVos SL, Nobuhara CK, Wegmann S, Roe AD, et al. Seed-  
569 competent high-molecular-weight tau species accumulates in the cerebrospinal fluid  
570 of Alzheimer's disease mouse model and human patients. *Ann Neurol*. 2016;80:355–  
571 67.
- 572 27. Saijo E, Ghetti B, Zanusso G, Oblak A, Furman JL, Diamond MI, et al. Ultrasensitive and  
573 selective detection of 3-repeat tau seeding activity in Pick disease brain and  
574 cerebrospinal fluid. *Acta Neuropathol (Berl)*. 2017;133:751–65.
- 575 28. Saijo E, Metrick MA, Koga S, Parchi P, Litvan I, Spina S, et al. 4-Repeat tau seeds and  
576 templating subtypes as brain and CSF biomarkers of frontotemporal lobar  
577 degeneration. *Acta Neuropathol (Berl)*. 2020;139:63–77.
- 578 29. Shi J, Aiken C. Saturation of TRIM5 $\alpha$ -mediated restriction of HIV-1 infection depends on  
579 the stability of the incoming viral capsid. *Virology*. 2006;350:493–500.
- 580 30. Hatzioannou T, Cowan S, Goff SP, Bieniasz PD, Towers GJ. Restriction of multiple  
581 divergent retroviruses by Lv1 and Ref1. *EMBO J*. 2003;22:385–94.

- 582 31. Wang Y, Balaji V, Kaniyappan S, Krüger L, Irsen S, Tepper K, et al. The release and trans-  
583 synaptic transmission of Tau via exosomes. *Mol Neurodegener.* 2017;12:5.
- 584 32. Tardivel M, Bégard S, Bousset L, Dujardin S, Coens A, Melki R, et al. Tunneling nanotube  
585 (TNT)-mediated neuron-to neuron transfer of pathological Tau protein assemblies.  
586 *Acta Neuropathol Commun.* BioMed Central; 2016;4:1–14.
- 587 33. Skachokova Z, Martinisi A, Flach M, Sprenger F, Naegelin Y, Steiner-Monard V, et al.  
588 Cerebrospinal fluid from Alzheimer’s disease patients promotes tau aggregation in  
589 transgenic mice. *Acta Neuropathol Commun.* 2019;7:72.
- 590 34. Ahmed Z, Cooper J, Murray TK, Garn K, McNaughton E, Clarke H, et al. A novel in vivo  
591 model of tau propagation with rapid and progressive neurofibrillary tangle pathology:  
592 the pattern of spread is determined by connectivity, not proximity. *Acta Neuropathol*  
593 *(Berl).* 2014;127:667–83.
- 594 35. Furcila D, Domínguez-Álvaro M, DeFelipe J, Alonso-Nanclares L. Subregional Density of  
595 Neurons, Neurofibrillary Tangles and Amyloid Plaques in the Hippocampus of Patients  
596 With Alzheimer’s Disease. *Front Neuroanat [Internet]. Frontiers*; 2019 [cited 2020 Apr  
597 22];13. Available from:  
598 <https://www.frontiersin.org/articles/10.3389/fnana.2019.00099/full>
- 599 36. Lace G, Savva GM, Forster G, de Silva R, Brayne C, Matthews FE, et al. Hippocampal  
600 tau pathology is related to neuroanatomical connections: an ageing population-based  
601 study. *Brain.* Oxford Academic; 2009;132:1324–34.
- 602 37. Zolotukhin S, Byrne BJ, Mason E, Zolotukhin I, Potter M, Chesnut K, et al. Recombinant  
603 adeno-associated virus purification using novel methods improves infectious titer and  
604 yield. *Gene Ther.* 1999;6:973–85.
- 605 38. Schindelin J, Arganda-Carreras I, Frise E, Kaynig V, Longair M, Pietzsch T, et al. Fiji: an  
606 open-source platform for biological-image analysis. *Nat Methods.* 2012;9:676–82.  
607  
608

609 **Figures**



610

611 **Figure 1: OHSCs maintain cellular diversity and display no spontaneous tau pathology.**

612 **a.** OHSCs from mice transgenic for P301S tau were fixed after 2 weeks in culture and stained

613 for nuclei (DAPI), the neuronal marker Map2, the astrocyte marker Gfap, and the microglial

614 marker Iba1. Scale bars are 50  $\mu$ m. **b.** OHSCs from P301S tau transgenic mice are positive

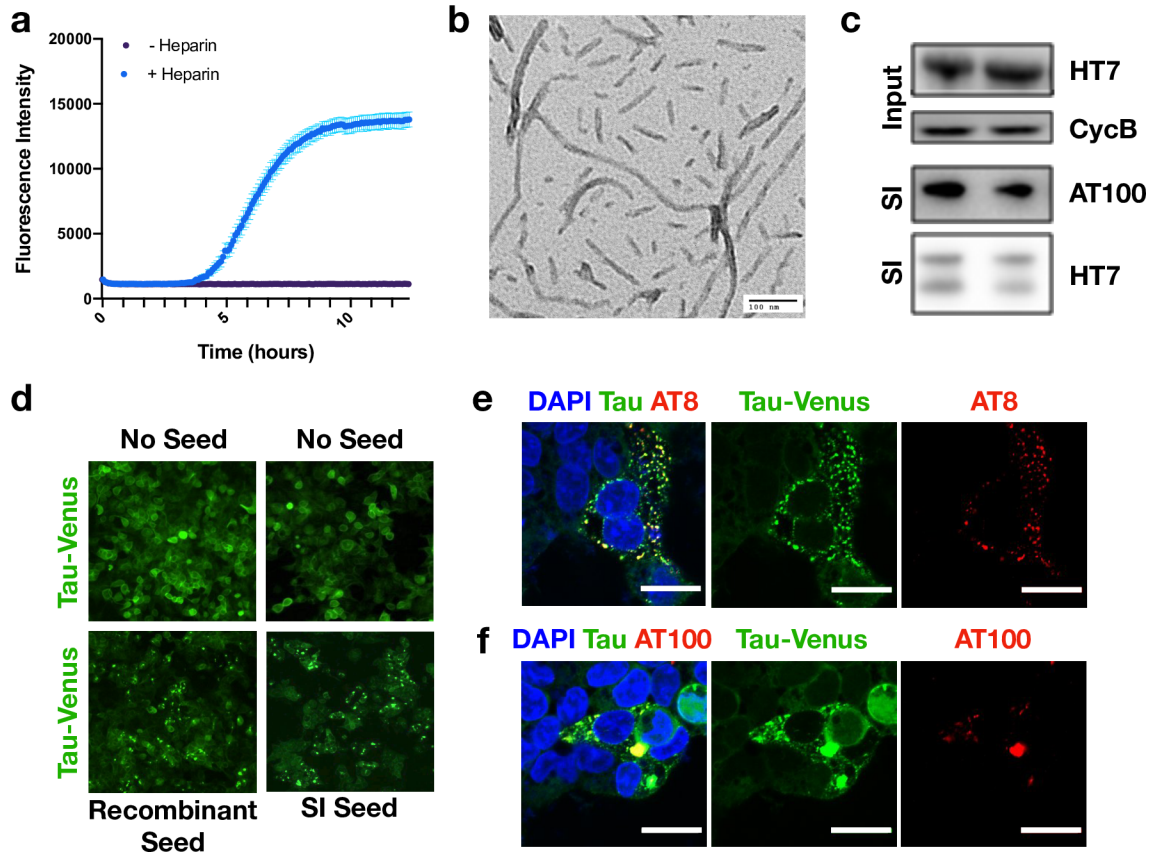
615 for human tau-specific antibody HT7 whereas OHSCs from WT mice are not. Scale bars 250

616  $\mu$ m and 25  $\mu$ m. **c.** OHSCs from P301S tau transgenic mice after 5 weeks in culture display

617 only background levels of staining with the phospho-tau specific antibody AT8. Slices were

618 stained with DAPI and Map2 as above and with pan-tau. Scale bars are 250  $\mu$ m.



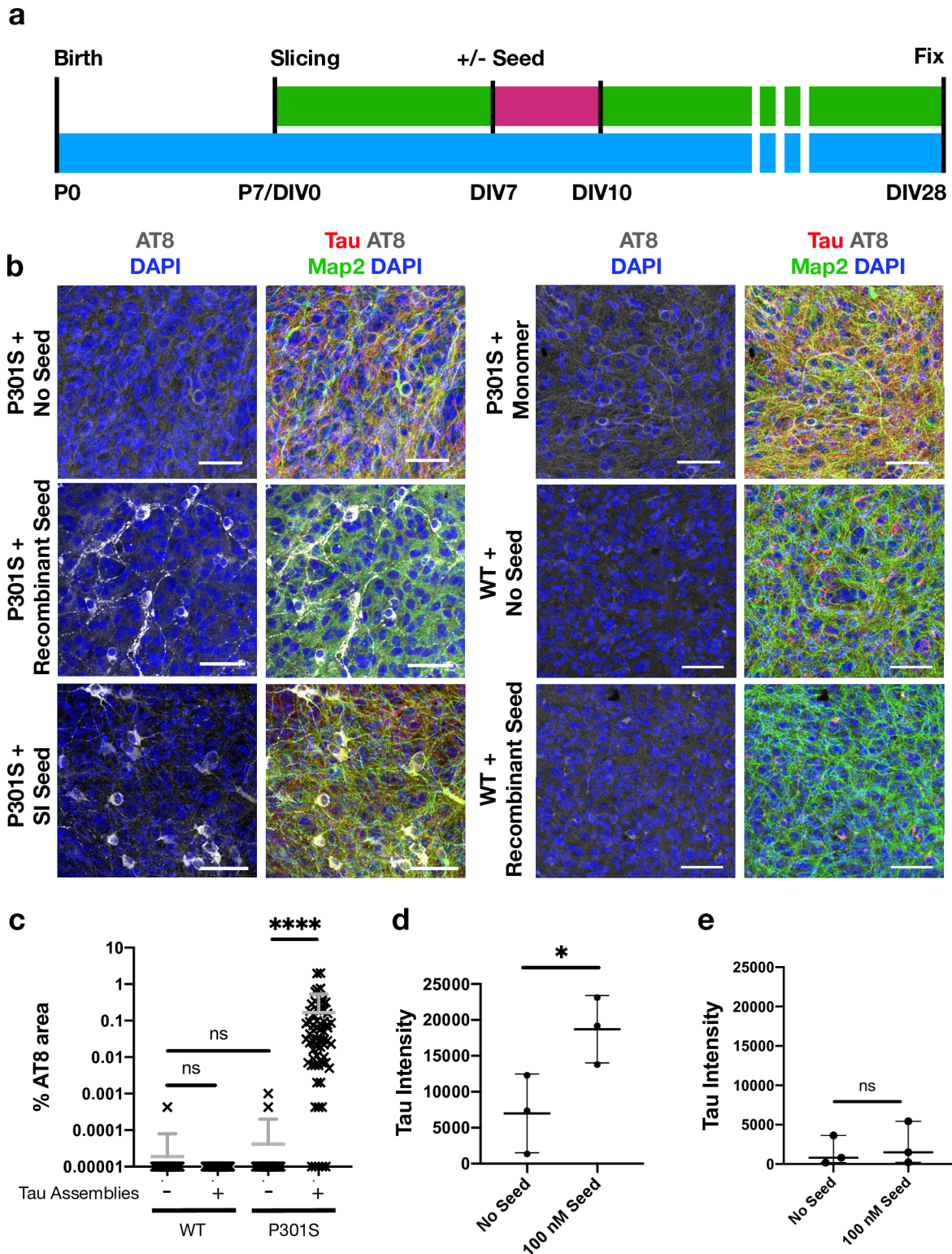


619

620 **Figure 2: Characterisation of tau assemblies.**

621 **a.** Aggregation kinetics for recombinantly produced P301S tau, monitored by ThT  
622 fluorescence. **b.** Representative TEM image of recombinantly produced P301S tau  
623 assemblies, aggregated with heparin. **c.** Aged P301S tau transgenic mouse brain homogenate  
624 was immunoblotted for human tau (HT7 antibody) to detect P301S tau and with Cyclophilin B  
625 which served as a loading control. Presence of SI tau was confirmed with HT7 (total tau) and  
626 AT100 (tau phosphorylated at pT212, pT214). Lanes represent homogenate and SI fractions  
627 from different mice which were subsequently pooled. **d.** Representative images from the tau-  
628 venus seeding assay 48 h after challenge with either recombinant P301S tau assemblies or  
629 SI tau in the presence of LF2000. **e,f.** Tau-venus aggregates observed following challenge  
630 with tau assemblies stain with AT8 and AT100 demonstrating that the induced tau aggregates  
631 are phosphorylated. Scale bars are 20  $\mu$ m.

632



633

634 **Figure 3: Challenging OHSCs with exogenous tau assemblies induces seeded tau**  
 635 **aggregation.**

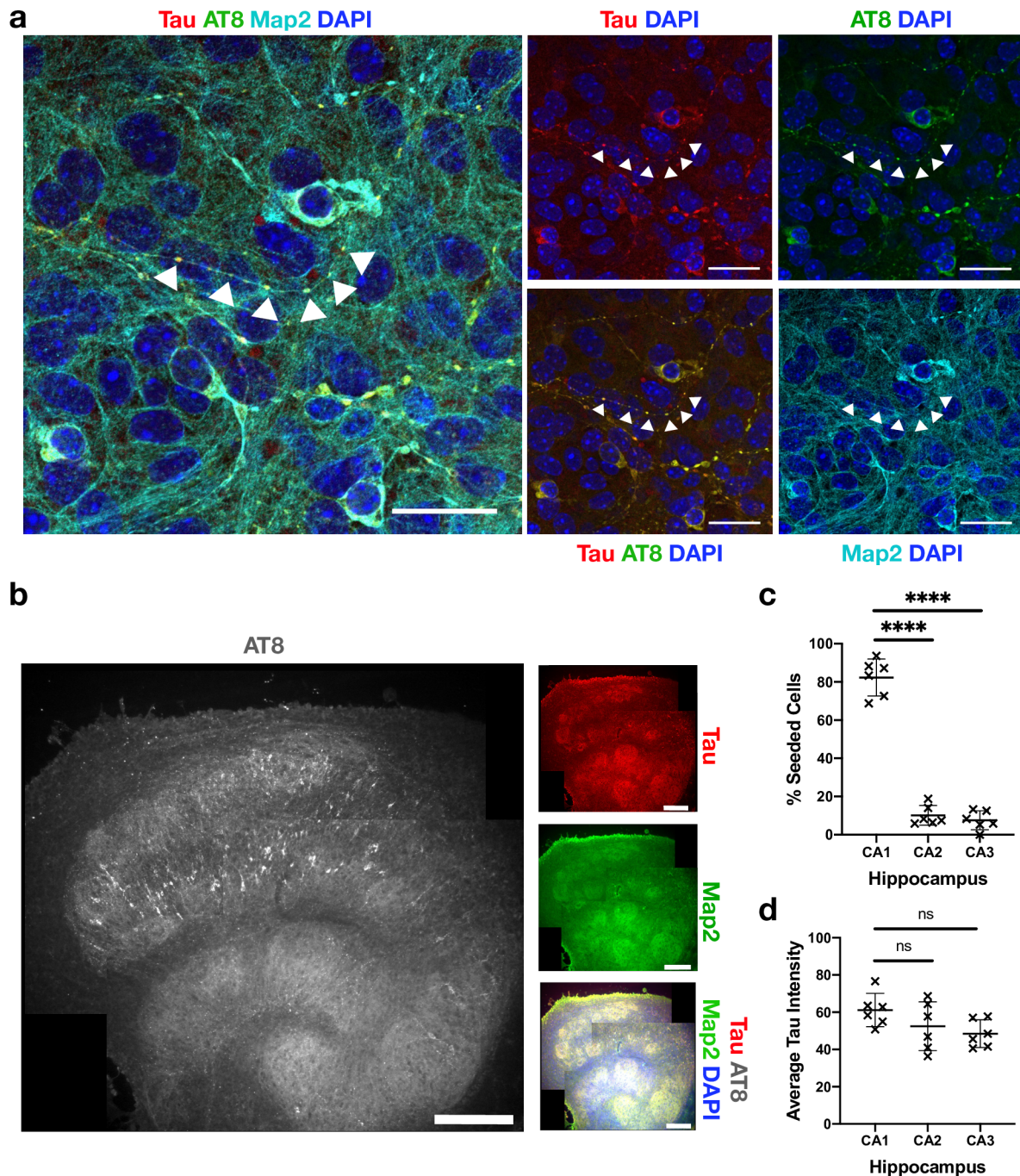
636 **a.** Schematic of OHSC preparation and treatment. Slices were prepared from P7 pups. Tau assemblies  
 637 were added to the media and incubated for 72 h. A complete media change was carried out at the end  
 638 of the seeding period (pink). At other times (green) 50% media changes were performed twice weekly  
 639 until fixation at 28 days *in vitro* (DIV). **b.** P301S OHSCs were challenged with either 100 nM



640 recombinant tau assemblies, 100 nM monomeric tau, 5  $\mu$ L of SI tau or buffer only. WT OHSCs were  
641 challenged with 100 nM recombinant tau assemblies or buffer only. Scale bars are 50  $\mu$ m. **c.**  
642 Quantification of seeding levels in WT and P301S OHSCs, upon the addition of 100 nM recombinant  
643 tau assemblies or buffer only. Statistical significance determined by Kruskal-Wallis Test by ranks and  
644 Dunn's multiple comparisons test (Slices from 3 different mice, per condition. \*\*\*\*  $P < 0.0001$ ). **d.**  
645 Analysis of the SI fraction of P301S OHSCs with and without the addition of 100 nM recombinant tau  
646 assemblies. **e.** Analysis of the SI fraction of WT OHSCs with and without the addition of 100 nM  
647 recombinant tau assemblies. Data normalised to overall levels of tau and loading control. Statistical  
648 significance determined by unpaired t-test with Welch's correction (Slices from 3 different mice, per  
649 condition. \*  $P < 0.05$ ).

650

651



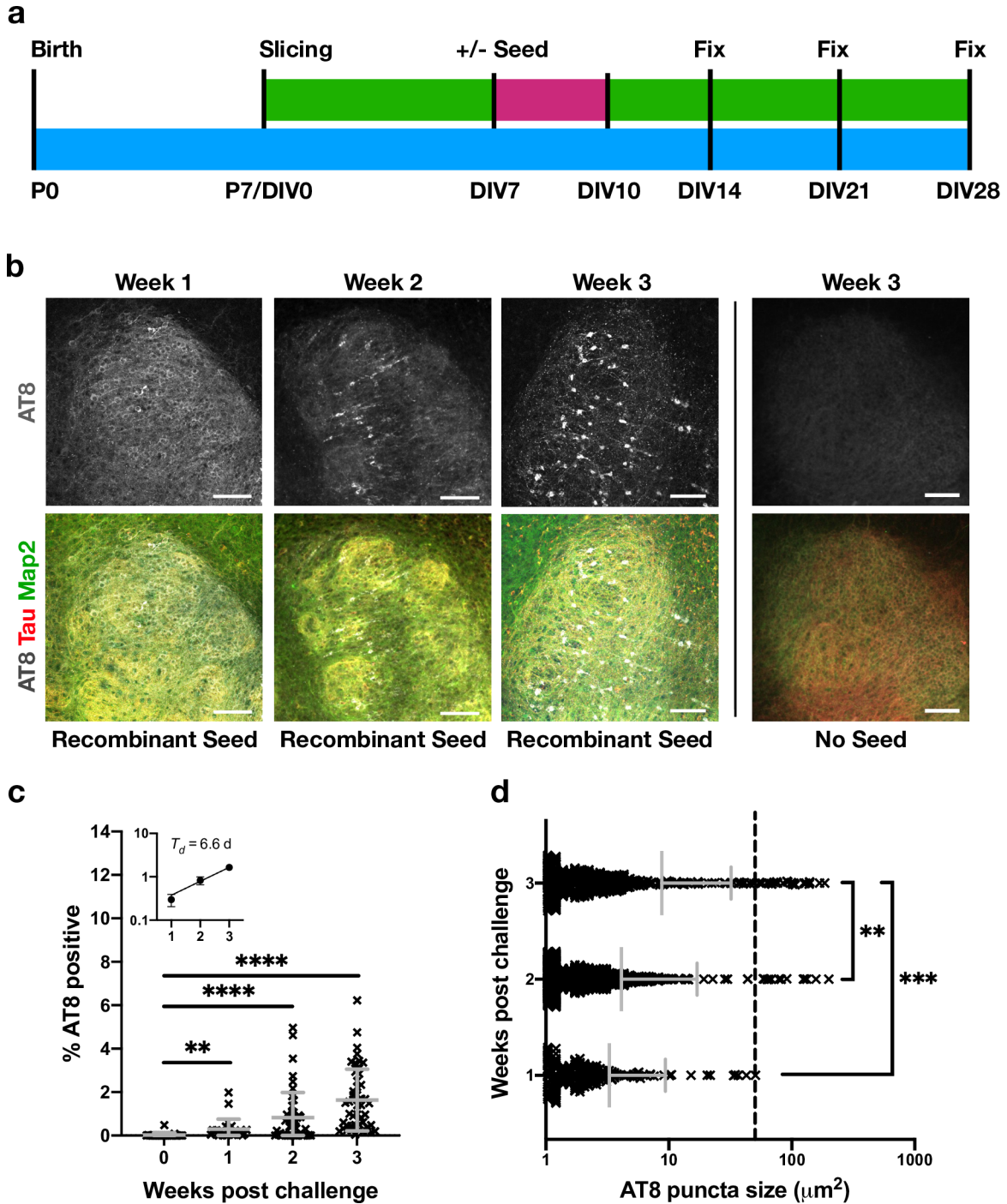
652

653 **Figure 4: Neurons display phospho-tau aggregates within intact nerve processes and**  
 654 **aggregates localise to CA1.**

655 **a.** OHSCs were challenged with 100 nM recombinant tau assemblies to induce seeded  
 656 aggregation. Hyperphosphorylated tau puncta can be observed along intact nerve processes  
 657 (arrows) and within cell bodies. Scale bars are 25  $\mu$ m. **b.** Tiled image of representative OHSC  
 658 challenged with 100 nM recombinant tau assemblies displays AT8 immunoreactivity  
 659 predominantly in the CA1 subregion. Scale bars are 250  $\mu$ m. **c.** The distribution of seeded  
 660 cells in hippocampal subregions was quantified by counting cells positive for AT8 aggregates.

661 **d.** Levels of tau, as quantified by pan-tau staining, show that CA1, CA2 and CA3 express  
662 similar levels of tau. Statistical significance determined by one-way ANOVA and Tukey's post  
663 hoc multiple comparisons test (multiple fields imaged from slices from 6 different mice. \*\*\*\*  
664  $P < 0.0001$ ).

665



666

667 **Figure 5: Phospho-tau reactivity and hyperphosphorylated tau aggregates increase**  
 668 **over time.**

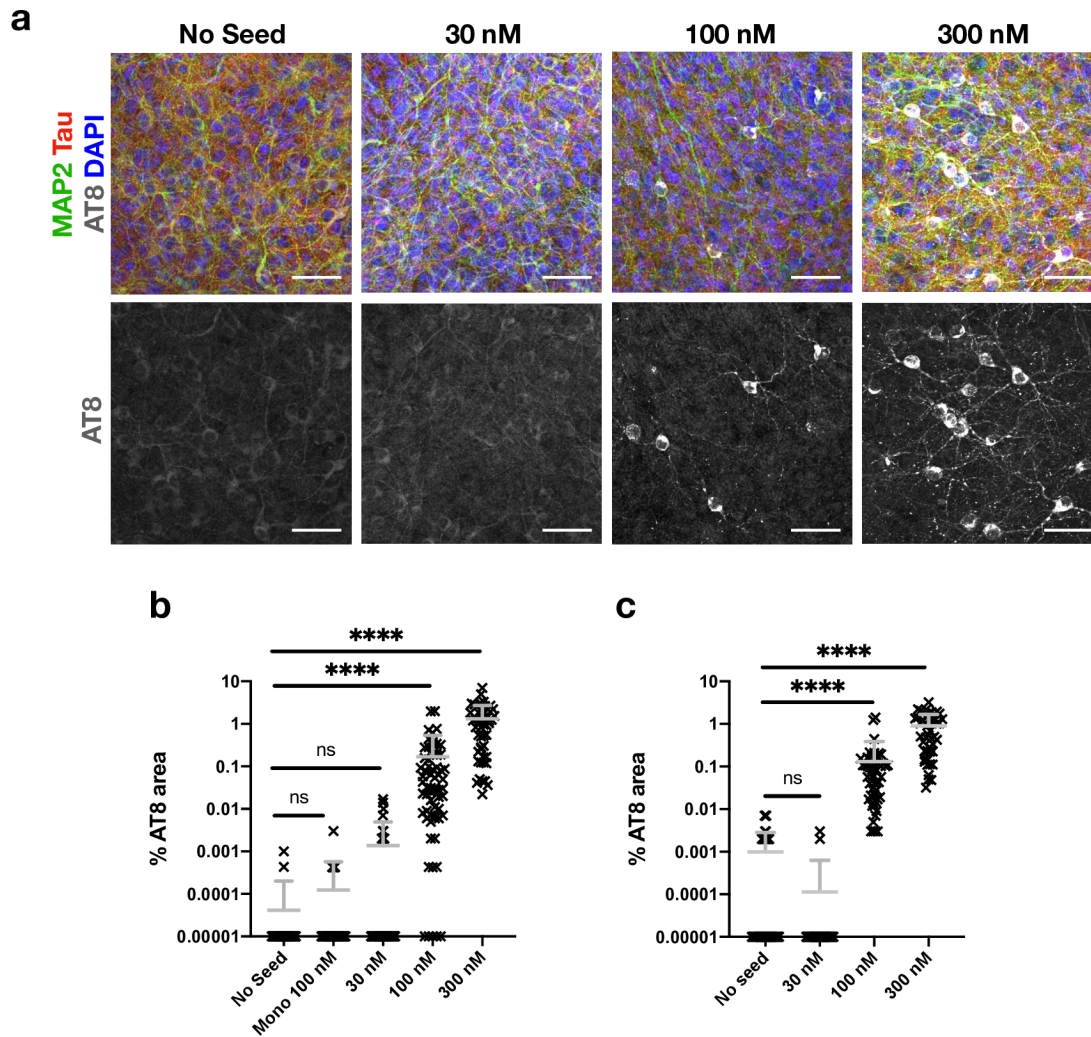
669 **a.** Schematic of OHSC preparation. 100 nM recombinant tau assemblies were added to the  
 670 media as previous and left for 72 hours (pink) followed by a complete media change.  
 671 Subsequently 50% media changes were performed twice weekly (green) until fixation at 1, 2  
 672 or 3 weeks post challenge. **b.** Slices fixed at 1 week post challenge display diffuse AT8  
 673 staining. Slices fixed at 2 or 3 weeks demonstrate increasing levels of puncta in cell bodies

674 and neurites. OHSCs not challenged with exogenous tau fibrils exhibit only diffuse background  
675 levels of AT8 reactivity. Scale bars are 100  $\mu\text{m}$ . **c.** Quantification of percent area that was AT8  
676 reactive shows a significant increase in phospho-tau levels, with a doubling time of  $\sim 7$  days.  
677 Statistical significance determined by Kruskal-Wallis Test by ranks and Dunn's multiple  
678 comparisons test (multiple fields imaged from slices from  $>2$  different mice per time point.  
679  $**P<0.01$ ,  $**** P<0.0001$ ). Inset represents the same data from weeks 1-3 plotted on a  
680 logarithmic scale. **d.** Quantification of AT8 positive puncta size shows an increase in the size  
681 of AT8 positive aggregates. Dotted line at 50  $\mu\text{m}^2$  represents approximate lower size limit of  
682 cell body-occupying lesions. Statistical significance determined by Kruskal-Wallis Test by  
683 ranks and Dunn's multiple comparisons test (multiple fields imaged from slices from  $>2$   
684 different mice per time point,  $**P<0.01$ ,  $***P<0.001$ ).

685

686



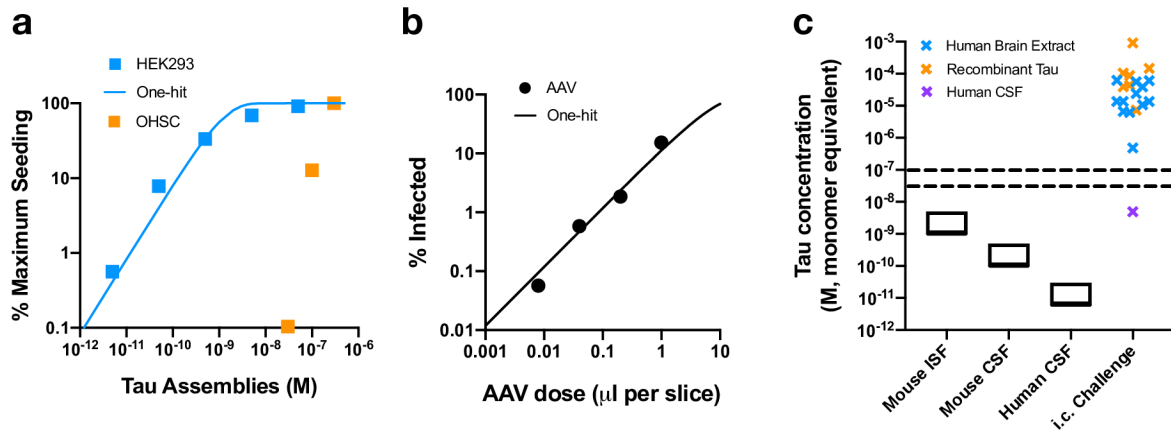


687

688 **Figure 6: Seeding of tau occurs with an apparent threshold**

689 **a.** OHSCs challenged with 30 nM, 100 nM and 300 nM of recombinant tau assemblies, or with  
690 buffer only. Scale bars are 50  $\mu$ m. **b.** Quantification of seeding levels in P301S OHSCs, upon  
691 the addition of 30 nM, 100 nM or 300 nM recombinant tau assemblies, 100 nM tau monomer  
692 or buffer only underneath the culture insert. Statistical significance determined by Kruskal-  
693 Wallis Test by ranks and Dunn's multiple comparisons test (Slices from 3 different mice, per  
694 condition. \*\*\*\* P<0.0001). **c.** Quantification of seeding levels in P301S OHSCs, upon the  
695 addition of recombinant tau assemblies or buffer only to the apical surface of individual slices.  
696 Statistical significance determined by Kruskal-Wallis Test by ranks and Dunn's multiple  
697 comparisons test (Slices from 3 different mice, per condition. \*\*\*\* P<0.0001).

698



699

700 **Figure 7: Tau seeding does not conform to one-hit dynamics**

701 **a.** Tau assemblies were titrated on HEK293 tau-venus cells using LF2000 transfection  
702 reagent, and the amount of seeding was quantified and expressed as percent of maximum. A  
703 one-hit curve was fitted using values outside the plateau. Tau seeding in OHSCs, means  
704 derived from Fig 6b, cannot be fitted to a one-hit model. **b.** Infection of P301S OHSCs with  
705 AAV1/2.hSyn-GFP with one-hit curve fitted to all data points (Slices from 3 different mice, per  
706 condition). **c.** Comparison of the concentration of tau used in stereotaxic injection experiments,  
707 coloured by origin, with ranges of ISF and CSF concentrations of tau measured in mice and  
708 humans, sourced from the literature (see Supp Table 1). The dotted lines represent the  
709 apparent threshold for the seeded aggregation of tau in neural tissue observed here at  
710 between 30-100 nM tau.

711